



Walter+Eliza Hall
Institute of Medical Research

Institute Research Publication Repository

This is the authors' accepted version of their manuscript accepted for publication in
Nature Chemical Biology.

The published article is available from Nature Publishing Group:

Lessene G, Czabotar PE, Sleebs BE, Zobel K, Lowes KN, Adams JM, Baell JB, Colman PM, Deshayes K, Fairbrother WJ, Flygare JA, Gibbons P, Kersten WJA, Kulasegaram S, Moss RM, Parisot JP, Smith BJ, Street IP, Yang H, Huang DCS, Watson KG. Structure-guided design of a selective BCL-XL inhibitor. *Nature Chemical Biology*. 2013 9(6):390-397. doi:10.1038/nchembio.1246

<http://www.nature.com/nchembio/journal/v9/n6/full/nchembio.1246.html>

Structure-guided design of a selective BCL-X_L inhibitor

Guillaume Lessene^{1,2*}, Peter E Czabotar^{2,3†}, Brad E Sleebs^{1,2†}, Kerry Zobel⁴, Kym L Lowes^{1,2}, Jerry M Adams^{2,5}, Jonathan B Baell^{1,2,6}, Peter M Colman^{2,3}, Kurt Deshayes⁴, Wayne J Fairbrother⁴, John A Flygare⁷, Paul Gibbons⁷, Wilhelmus J A Kersten^{1,2}, Sanji Kulasegaram^{1,2,8}, Rebecca M Moss^{1,2}, John P Parisot^{1,2,9}, Brian J Smith^{1,2,10}, Ian P Street^{1,2}, Hong Yang^{1,2}, David C S Huang^{1,2}, Keith G Watson^{1,2}

Address

¹Chemical Biology Division, The Walter and Eliza Hall Institute of Medical Research, Parkville, Victoria 3052, Australia.

²Department of Medical Biology, The University of Melbourne, Parkville, Victoria 3010, Australia.

³Structural Biology Division, The Walter and Eliza Hall Institute of Medical Research, Parkville, Victoria 3052, Australia.

⁴Department of Early Discovery Biochemistry, Genentech, Inc., South San Francisco, California 94080, United States.

⁵Molecular Genetic of Cancer Division, The Walter and Eliza Hall Institute of Medical Research, Parkville, Victoria 3052, Australia, Australia.

⁶Current address: Monash Institute of Pharmaceutical Sciences, Parkville, Victoria 3052, Australia.

⁷Department of Discovery Chemistry, Genentech, Inc., South San Francisco, California 94080, United States.

⁸Current address: Chemistry Department, Monash University, Clayton, Victoria, Australia.

⁹Current address: Peter McCallum Cancer Centre, East Melbourne, Victoria, Australia.

¹⁰Current address: Department of Chemistry, La Trobe Institute of Molecular Sciences, La Trobe University, Bundoora, Victoria 3086, Australia.

*email: glessene@wehi.edu.au.

†These authors contributed equally to this work

ABSTRACT

The pro-survival BCL-2-family protein, BCL-X_L, is often over-expressed in solid tumors and renders malignant tumor cells resistant to anti-cancer therapeutics. Enhancing apoptotic responses by inhibiting BCL-X_L will likely have widespread utility in cancer treatment and, compared to inhibiting multiple pro-survival BCL-2 family members, a BCL-X_L-selective inhibitor would be expected to minimize the toxicity to normal tissues. We describe the discovery by a high throughput screen of a novel series of small molecules targeting BCL-X_L and their structure-guided development by medicinal chemistry. The optimized compound, **WEHI-539**, has high affinity (sub-nM) and selectivity for BCL-X_L and potently kills cells by selectively antagonizing its pro-survival activity. **WEHI-539** will be an invaluable tool for distinguishing the roles of BCL-X_L from those of its pro-survival relatives, both in normal cells and crucially in malignant tumor cells, many of which may prove to rely upon BCL-X_L for their sustained growth.

As the evasion of apoptosis is critical for cancer development and imposes a major barrier to effective therapy, reinstating the apoptotic response selectively in tumor cells is a compelling therapeutic goal¹. The major gateway to apoptosis is guarded by BCL-2 and its pro-survival relatives, such as BCL-X_L and MCL-1, which are strongly implicated in tumor development and the resistance to diverse cytotoxic therapies^{2,3}. To date only a few compounds targeting these proteins have progressed to clinical development⁴, due to the challenges associated with targeting protein-protein interactions^{5,6}.

We sought to develop a specific inhibitor of BCL-X_L, a protein over-expressed in certain cancers⁷ and strongly implicated as a chemoresistance factor⁸. Like BCL-2⁹, BCL-X_L acts to counter apoptosis (programmed cell death), and its overexpression in tumors confers a strong survival advantage by antagonizing signals that would normally induce cell death (e.g. deregulated expression of c-MYC¹⁰).

Members of the BCL-2 protein family are the key regulators of the intrinsic apoptotic pathway¹¹ and their interactions determine whether a cell lives or dies. Pro-survival proteins like BCL-X_L keep cells alive by preventing activation of the cell death mediators BAX and BAK, one or both of which are required for the execution phase of apoptosis¹². Cellular stresses, such as those induced by oncogenic proteins or chemotherapeutic agents, trigger apoptosis by activating pro-apoptotic BH3-only proteins (e.g. BIM, BAD, NOXA), the natural antagonists of BCL-X_L and its relatives. They initiate apoptosis by binding to and inhibiting their pro-survival relatives, and some also directly activate BAX and BAK to unleash mitochondrial outer membrane permeabilization^{13,14}. The BH3-only proteins function primarily by inserting their BH3 domain, an amphipathic α -helix of ~26 residues, into a long shallow groove on the surface of the pro-survival proteins.

In many tumors, elevated levels of proteins like BCL-X_L raise the barrier to apoptosis. Restoring the apoptotic response with compounds mimicking the BH3-only proteins is therefore an attractive approach for developing novel cancer therapies⁴. The potential of such 'BH3 mimetics' for treating cancer is supported by proof-of-concept studies with peptidyl ligands and small organic compounds^{15,16} and by recent early phase clinical studies¹⁷⁻²⁰. The most advanced BH3 mimetic in the clinic is ABT-263 (navitoclax), developed by AbbVie^{21,22}, which is showing promise in the treatment of certain lymphoid malignancies, especially chronic lymphocytic leukemia¹⁹. Functionally, ABT-263 (like ABT-737, the pre-clinical proof-of-concept compound) binds tightly to several pro-survival proteins. Novel BH3 mimetics with narrower target specificity may help determine the role of each pro-survival protein in driving therapeutic responses, and prevent the current limitations to dosing with ABT-263 (e.g. neutropenia)^{19,23}.

These findings support our efforts to discover and develop a BCL-X_L-selective inhibitor. This task is particularly challenging, however, since the BCL-X_L interface to which BH3 domains bind is a large, highly lipophilic and shallow surface groove⁶. Though many BH3-only proteins have defined

target profiles (e.g. BAD targets BCL-2, BCL-X_L and BCL-W), no naturally occurring ligand exclusively targets BCL-X_L, raising questions about the feasibility of our goal. While a biomarker for a *bona fide* BCL-X_L inhibitor is platelet death, since their survival relies entirely on BCL-X_L^{24,25}, the paucity of appropriate biochemical and cellular assays that validate selective on-target activity has impeded the development of BH3 mimetics.

We report the discovery and development of a highly potent and selective BCL-X_L inhibitor series, based on a novel scaffold arising from a high-throughput chemical screen. Crystal structures of the inhibitors bound to BCL-X_L have guided their development and revealed the basis for their selective binding. By using genetically defined cells, we have validated their cellular mechanism of action. These results represent a major advance in BCL-2 protein targeting by demonstrating that exquisite selectivity for a single pro-survival protein can be achieved by a small molecule even with these highly challenging protein targets⁵. The optimal compound in the series, **WEHI-539**, should prove invaluable for probing the roles of BCL-X_L in normal physiology as well as determining its contribution to tumor maintenance.

RESULTS

Inhibiting BCL-X_L with a benzothiazole-hydrazone scaffold

A library of ~100,000 compounds²⁶ was screened against BCL-W, a close relative of BCL-X_L, and hits were validated by orthogonal binding assays; by their ability to disrupt BCL-X_L•BIMBH3-26mer or MCL-1•BIMBH3-26mer complexes (**Supplementary Results, Supplementary Fig. 1 and Supplementary Tables 1 and 2**). These analyses led to a lead compound series containing a benzothiazole-hydrazone core: Compound **1a** (**Fig. 1a**) clearly was a promising lead for BCL-X_L (IC₅₀ = 7.7 μM, **Supplementary Table 2**). Synthesis of close analogs rapidly yielded compound **1b** (**Fig. 1a**), with low micromolar activity for BCL-X_L (IC₅₀ = 2.2 μM, **Supplementary Table 3**).

Using compound **1b** as a lead compound, we developed a binding mode hypothesis (**Fig. 1b**) to guide a medicinal chemistry campaign to improve affinity. Structural studies show that the α -helical BH3 domains bind tightly to four hydrophobic pockets (P1 to P4) that constitute a groove on the surface of the pro-survival BCL-2 family members²⁷⁻²⁹. This binding is augmented by electrostatic interaction of a conserved arginine (ARG) residue on the pro-survival proteins (between P3 and P4) with a conserved aspartate (ASP) on the BH3 domain. Since P2 and P4 are particularly important for the association of BH3-peptides and pro-survival proteins, we reasoned that these two hydrophobic pockets on BCL-X_L likely mediate binding of our inhibitors and, due to its small size, compound **1b** could only occupy one of these pockets (**Fig. 1b**). Therefore, extending compound **1b** should allow it to reach a second interaction site. Additionally, we hypothesised that the carboxylic acid in compound **1b** interacts with the conserved ARG139 in the BCL-X_L groove.

With this model in mind, we prepared a series of acylsulfonamide derivatives of **1b** to explore extensions towards a second binding pocket. The best analog within this series, compound **2** (**Fig. 1c**), afforded an X-ray crystal structure of the complex, establishing the binding mode of our series (see **Supplementary Table 4** for crystallographic data). Extension of compound **2** allowed interaction with the P4 pocket (**Supplementary Fig. 2**), though this interaction occurred with the binding site in a second BCL-X_L molecule, rather than that binding the benzothiazole core. This crossed dimeric structure likely facilitated nucleation of the crystals, as this dimer is not present in solution (**Supplementary Fig. 3**). Rather, the P4 extension in compound **2** is flexible enough to shift between a bound and unbound conformation, thus providing only a moderate increase in affinity over compound **1b** (IC₅₀ = 0.77 and 2.2 μ M, respectively).

The structure revealed a remarkable shape complementarity between the core molecule from our screen and the hydrophobic P2 pocket of BCL-X_L (**Figs. 1d and 1e**). Specifically, the benzothiazole-hydrazone moiety of compound **2** fits snugly into the deep hydrophobic pocket generated by

displacement of the PHE105 side chain (**Fig. 1d**), which forms the base of P2 in apo-BCL-X_L. This deeper P2 pocket does not exist in complexes between BCL-X_L and BH3 peptides from BH3-only proteins³⁰, but PHE105 is similarly exposed in the complexes of BCL-X_L with the BH3 domains of BAK or BECLIN^{31,32} (**Supplementary Figs. 4a-c**). In contrast, the binding of ABT-737²⁹ pushes PHE105 deeper within the P2 pocket (**Supplementary Fig. 4d**). These varied results reinforce the idea that P2 possesses a high degree of plasticity that can be targeted by small molecules³³.

The BCL-X_L•compound **2** complex provided additional insights into the binding. The hydrophobic interactions within P2 are buttressed by two key hydrogen bonds: one between the backbone carbonyl of SER106 and the hydrazone NH, and another between the backbone NH of LEU108 and the benzothiazole ring nitrogen (**Fig. 1e**). Further along the groove, PHE105 flanks the biaryl section of compound **2** (**Fig. 1f**). Finally, as predicted, the acidic acylsulfonamide interacts with the guanidinium moiety of ARG139 (**Fig. 1f**). In contrast, ABT-737 does not interact with ARG139 in BCL-X_L²⁹.

We improved the affinity and ligand efficiency of compound **1b** by optimizing its core. Briefly, a broad Structure Activity Relationship (SAR) study found that replacing the furan ring with a phenyl ring and the terminal phenyl ring with either a picolinic acid or a thiazole acid both increased affinity and drug-likeness. Final optimization to lock the compounds in their binding conformation produced compounds **3** and **4** (**Fig. 2a**), which combine refinements to the core and display ~100-fold increased affinity over compound **1b** (**3**: IC₅₀ = 23 nM, **4**: IC₅₀ = 24 nM), with minimal increase in molecular weight (**Supplementary Table 3**). A full description of the medicinal chemistry effort to derive compounds **3** and **4** will be reported elsewhere.

X-ray structures of analog **3** confirmed a binding mode similar to compound **2** (**Fig. 2b**). It is likely that the increased affinity seen with compounds **3** and **4** reflects their improved positioning within P2 and along the hydrophobic groove. Notably, in these optimized analogs, the interaction of the

picolinic acid or thiazole acid with ARG139 is slightly modified and, not unexpectedly, engages their respective ring nitrogen atoms (**Supplementary Fig. 5**).

Highly potent BCL-X_L inhibitors *via* structurally enabled design

Structural insights from BCL-X_L complexes with compounds **2**, **3** and **4** pinpointed the most productive vectors towards P4 (sketched in **Fig. 2b**). We prepared a series of simple phenoxyalkyl extensions positioned ortho to the carboxylic acid on both the picolinic acid and thiazole acid series. Compounds **5** and **6** represent the best analogs in each series: a 5-atom extension from the picolinic acid and a 4-atom extension from the thiazole ring (**Figs. 2a and 2c**), showing a 4- and 10-fold increase in affinity over compounds **3** and **4** (**5**: IC₅₀ = 6.2 nM; **6**: IC₅₀ = 1.5 nM, **Supplementary Table 3**), respectively.

Finally, to form additional positive interactions with polar residues on the edge of pocket P4, we synthesised a small panel of substituted phenol derivatives based upon compound **6**. In the development of ABT-737, a dimethylaminoethyl group at this position increased affinity for BCL-X_L³⁴, and the X-ray structure of ABT-737•BCL-X_L shows the dimethylamino moiety interacting with GLU96²⁹. In our series, this directed strategy yielded compound **7 (WEHI-539)**, which displayed high affinity for BCL-X_L (IC₅₀ = 1.1 nM, **Fig. 3a**). As the lower limit for IC₅₀ determination in our primary AlphaScreen™ competition assay is approximately 1 nM, that assay did not clearly discriminate between **WEHI-539** and compound **6**. However, measurement of their dissociation constants (K_D) with BCL-X_L by SPR indicated that **WEHI-539** bound with higher affinity. Coupled with its superior cellular activity, **WEHI-539** was the optimal compound in our series (see Discussion and **Supplementary Table 3**). X-ray structures of compound **6 (Fig. 2c)** and **WEHI-539 (Fig. 3b)** show similar occupancy of the P2 hydrophobic pocket. As expected, the phenyl ring of compound **6** and the

phenoxy ring of **WEHI-539** occupy the P4 pocket of BCL-X_L, but the pocket surrounds **WEHI-539**'s benzylamino extension more snugly (compare **Figs. 2c** and **3b**). This P4 interaction is mainly hydrophobic, replacing several water molecules buried within this highly lipophilic pocket, as highlighted by the detailed structure of compound **3** bound to BCL-X_L (**Supplementary Fig. 6**).

Although the aminomethyl group on the phenoxy ring of **WEHI-539** enhanced its binding affinity and cellular activity, the structural basis of this improvement was initially less certain, because structures of **WEHI-539**•BCL-X_L revealed two slightly different binding modes. One structure – probably a crystallization artifact – shows a hydrogen bond between the benzylamine moiety and ethyleneglycol, whilst in the second the amino group forms a hydrogen bond with GLU96, as observed in the ABT-737•BCL-X_L complex (**Fig. 3c**). Comparison of ABT-737 and **WEHI-539** binding modes shows notable differences in their pose (**Fig. 3d**): because **WEHI-539** displaces PHE105, it engages the hydrophobic pocket P2 more deeply than ABT-737 or indeed most natural BH3 domains. Due to this enhanced interaction, and the engagement by its carboxylic acid group of ARG139, **WEHI-539** achieves very high affinity without the π -stacking seen in ABT-737's P4 extension²⁹.

WEHI-539 binds BCL-X_L tightly but distinctly from ABT-737 and BIM

To gain further insight into the interactions between BCL-X_L and compounds, we developed a direct binding assay using SPR (Biacore S51, GE) that allowed us to ascertain the stoichiometry, binding affinity and kinetics for the interaction of our compounds with the binding groove of BCL-X_L (**Online Methods** and **Supplementary Note 1**). This was achieved by comparing concomitant binding to BCL-X_L (total binding) and to BCL-X_L complexed with a high affinity BIM 26-mer peptide ($K_D = 0.2$ nM), which effectively blocked compound binding in the binding groove and thus reflects non-specific

binding (see **Supplementary Note 1**). Discriminating between specific and non-specific compound binding was critical in the early stages of the medicinal chemistry campaign, as some compounds (e.g. **1b**) exhibited both specific and non-specific BCL-X_L binding. As the affinity of our compound series increased from compound **1b** to **WEHI-539** (**Figs. 4a-d**), the non-selective binding component significantly decreased (compare **Supplementary Fig. 17a** through to **Supplementary Fig. 20a in Supplementary Note 1**).

Binding levels for each analog confirmed that the ligand and protein formed 1:1 complexes, excluding non-selective binding as the principal interaction in the primary AlphaScreen™ assay (**Supplementary Note 1**). Notably, although compound **2** ($K_D = 0.46 \mu\text{M}$) has higher affinity than compound **1b** ($K_D = 1.1 \mu\text{M}$, **Fig. 4a**), its association rate is significantly slower (**Fig. 4e**), perhaps because the flexible P4 extension increases the overall flexibility of the molecule. The lower dissociation rates of compounds **3** and **4** indicate the optimized fit with the protein produced more stable complexes (**3**: $K_D = 3.4 \text{ nM}$; **4**: $K_D = 8.8 \text{ nM}$, **Supplementary Table 3, Figs. 4b and 4e**). They also have higher association rates, presumably due to engagement of ARG139 by the picolinic and thiazole acids.

Finally, the increased affinities of compound **5** and **WEHI-539** ($K_D = 1 \text{ nM}$ and 0.6 nM , respectively, **Figs. 4d-e**) stem from another substantial decrease in dissociation rate. **WEHI-539** and **ABT-737** have comparable binding affinity ($K_D = 0.6 \text{ nM}$ and 0.4 nM , respectively, **Figs. 4d-f**), but **WEHI-539** exhibits faster association and dissociation rates than **ABT-737** (**Figs. 4e**). Compared to the **BIM-BH3** peptide ($K_D = 0.2 \text{ nM}$), **WEHI-539** associates slightly faster but also disassociates faster; thus **BIM** remains the highest affinity ligand for BCL-X_L.

Benzothiazole-hydrazone compounds selectively inhibit BCL-X_L

We assessed the selectivity of our compounds against the pro-survival proteins MCL-1, and BCL-W and found that compound **1a** already showed good selectivity for BCL-X_L (**Supplementary Table 2**). Notably, the tight ligand **WEHI-539** retains this selectivity (500 fold over BCL-2 and 400 fold over BCL-W, MCL-1 and A1, **Supplementary Tables 3** and **Supplementary Note 1**). This result was unexpected because BCL-X_L is more closely related to BCL-2 and BCL-W than to MCL-1 or A1³⁵. We suggest that the snug fit between the benzothiazole moiety and the P2 pocket of BCL-X_L, buttressed by an array of hydrogen bonds, confers this high selectivity.

WEHI-539 kills mouse embryonic fibroblasts that lack MCL-1

We next studied the activity of **WEHI-539** on cells and, in particular, we assessed whether it kills by direct inhibition of BCL-X_L. Several criteria against which selective inhibitors of the pro-survival proteins should be evaluated have been proposed^{4,36}. As well as very strong target protein(s) binding (**Supplementary Table 3**), these criteria include evidence that induced cell death (1) is apoptotic, (2) depends on BAX and/or BAK for cell killing, and (3) has biological activity consistent with the target selectivity profile. For example, ABT-737 causes platelet depletion due to BCL-X_L inhibition, whereas cells expressing high levels of MCL-1 are resistant to ABT-737^{24,37}. To date, only ABT-737 and its close relatives have fulfilled all these criteria^{4,38}.

To address these criteria, we determined whether our selective BCL-X_L inhibitors elicited apoptosis rather than non-specific cell death using wild-type mouse embryonic fibroblasts (MEFs) and matching MEFs lacking MCL-1, BCL-2 or BCL-X_L^{35,37,39}. Two hallmarks of apoptotic cell death, release of mitochondrial cytochrome *c* and caspase-3 processing, were evident in **WEHI-539**-treated cells (**Figs. 5a** and **5b**, **Supplementary Figs. 7** and **8**), but only if MCL-1 was absent. Furthermore, blocking caspase activity using the pan-caspase inhibitor qVD-OPh abrogated killing by **WEHI-539** in

MCL-1-deficient MEFs (**Supplementary Figs. 9**). As anticipated^{37,39}, the presence of MCL-1 blocked apoptosis induction by **WEHI-539**, as well as by ABT-737, confirming the target specificity of **WEHI-539** (**Supplementary Fig. 10**).

To ascertain whether the cell-based activity reflected binding to BCL-X_L, we assessed the ability of compounds **3**, **5** and **WEHI-539** to kill MCL-1-deficient MEFs (**Fig. 5c**). Encouragingly, the cell-based activity strongly correlated with binding affinity for BCL-X_L (**Fig. 5d**). Higher serum concentrations reduced **WEHI-539** activity, as observed with ABT-737, probably reflecting decreased cellular uptake due to serum protein–compound binding (**Supplementary Fig. 11**)¹⁶.

Since MCL-1-deficient MEFs require BCL-X_L for survival (**Supplementary Fig. 10**), our evidence that **WEHI-539** induces apoptosis in MEFs only if they lack MCL-1 supports the notion that cell killing induced by **WEHI-539** is due to direct inhibition of BCL-X_L. Accordingly, restoring expression of MCL-1 in *mcl-1* knockout cells renders them highly resistant to **WEHI-539** (**Supplementary Fig. 12**). Notably, while **WEHI-539** and ABT-737 are equipotent when BCL-X_L is over-expressed in MEF cells, ABT-737 is strikingly more effective (EC₅₀ = 2.5 nM) than **WEHI-539** (EC₅₀ = 0.48 μM) against cells over-expressing BCL-2 (**Supplementary Fig. 12**), consistent with our biochemical evidence that **WEHI-539** is a poor antagonist of BCL-2 (**Supplementary Table 3**).

WEHI-539 induces BAK-mediated apoptosis in MEFs

We used another set of engineered cell lines to prove definitively that **WEHI-539** acts specifically on BCL-X_L and not its relatives, especially the closely related BCL-2. These studies exploited the observation³⁹ that the cell death mediators BAX and BAK are differentially controlled: BAX is regulated by multiple pro-survival BCL-2 family members (including BCL-X_L and BCL-2) but BAK is principally regulated by BCL-X_L and MCL-1 (**Fig. 6a**). In the absence of MCL-1, a BCL-X_L inhibitor should drive apoptosis in a manner that requires BAK, but not BAX. Accordingly, we assessed the

impact of the BH3 mimetics on fibroblasts that only express BAX or BAK, or fibroblasts lacking both BAX and BAK, with the MCL-1 in these cells inactivated by a selective BH3 peptide ligand, BIM2A⁴⁰. While ABT-737 could kill cells that expressed either BAX or BAK^{37,41}, **WEHI-539** could only kill cells that contained BAK (**Fig. 6b**). This observation was confirmed in MEFs where MCL-1 activity and levels were abrogated by expression of its natural and selective BH3-only ligand NOXA (**Supplementary Fig. 13**). Cytochrome *c* release and caspase-3 processing confirmed that **WEHI-539** induces apoptosis in BAX-deficient MEF cells expressing BIM2A, but not in their BAK-deficient counterparts (**Figs. 6c-d, Supplementary Figs. 14-15**). At the molecular level, the failure of **WEHI-539** to kill MEF cells lacking BAK could not be explained by an inability of **WEHI-539** to disrupt the BCL-X_L•BAX complex (**Supplementary Table 5**). **WEHI-539**'s dependency on BAK to kill cells proves that it lacks significant ability to target BCL-2 or BCL-W, since they are the pro-survival proteins that constrain BAX but not BAK (**Fig. 6a**). As expected of functional BH3 mimetics, neither **WEHI-539** nor ABT-737 killed cells lacking both BAX and BAK, even when MCL-1 was inhibited by BIM2A (**Fig. 6b**) or NOXA (**Supplementary Fig. 13**).

WEHI-539 induces platelet apoptosis

As platelets depend exquisitely on BCL-X_L for their survival^{24,25,42}, we evaluated the ability of our inhibitors to induce platelet death. Genetic loss of BCL-X_L²² or pharmacological inhibition of BCL-X_L with ABT-737 or its relatives (e.g. ABT-263) causes thrombocytopenia (low circulating platelet numbers) *in vivo*¹⁹.

Strikingly, **WEHI-539** efficiently triggered the killing of platelets purified from mice (**Fig. 6e**) or humans in culture (**Fig. 6f**). This death was blocked by a broad-spectrum caspase inhibitor (qVD-OPh) (**Fig. 6f**) and ameliorated in platelets with reduced levels of BAX and BAK (**Fig. 6e**) – note that studies with *bax*^{-/-}*bak*^{-/-} platelets could not be readily performed since these mice are not viable¹². These studies

demonstrate that **WEHI-539** triggers apoptosis in platelets. Since **WEHI-539** targets only BCL-X_L and not any other pro-survival proteins, our observations support the conclusion that platelets rely only on BCL-X_L, for their survival¹².

DISCUSSION

Targeting the interactions between BCL-2 family proteins has garnered great interest, but developing drug-like compounds with high and selective affinity for the long and shallow BH3-binding grooves on pro-survival BCL-2-like proteins is difficult. Several critical issues attend attempts to target PPIs in general, and BCL-2-family proteins in particular: a) *compound size*: As protein interaction faces are usually extensive, are large ligands (> 500 D) essential to interfere effectively with their function? b) *selectivity*: ABT-263 and ABT-737 target more than one pro-survival BCL-2 family member with very high affinity – can more selective inhibitors be developed? c) *validation of on-target activity*: The numerous reported putative BCL-2 family inhibitors that remain unconfirmed⁴ stresses the need for proper biological validation.

Our study provides insights on all these issues. Firstly, compounds **3** and **4** show that relatively potent BCL-X_L inhibitors can be developed that retain low molecular weight (<450 D), but only the compounds with much greater affinity, namely **5**, **6** and **WEHI-539**, proved effective in cellular assays. This improvement, obtained by extending the compounds from P2 into the P4 hydrophobic pocket, required a moderate gain in molecular weight (e.g. from MW = 420 for compound **4** to MW = 584 for **WEHI-539**). High molecular weight can prove a challenge for drug development by increasing metabolic liabilities and leading to poor oral availability⁴³, although ABT-263 at MW = 975 shows that such sizes need not be a barrier. Serum binding did limit the activity of some of our larger compounds (**Supplementary Fig. 9**), as with some ABT-737 precursors^{16,21}, and may well be a common obstacle in targeting PPIs, especially those involving hydrophobic interfaces. Regardless, we observed, as in the

ABT-737 series, that a free amine in the P4-binding region of **WEHI-539** allowed robust cellular activity even in high serum concentrations.

Our study presents an entirely novel scaffold discovered through high-throughput chemical screening and describes its development through structure-guided medicinal chemistry into a ligand, **WEHI-539**, with more than a 400-fold higher affinity for BCL-X_L versus other pro-survival BCL-2 family members, distinguishing it from other well-characterized inhibitors, such as ABT-737 (which binds to BCL-X_L, BCL-2 and BCL-W). Indeed, it represents the first truly specific synthetic ligand for BCL-X_L (A-385358 from AbbVie bound preferentially to BCL-X_L but still retained <100 nM affinity for BCL-2⁴⁴). Hence, **WEHI-539** will be a powerful tool for studies on the biochemical and biological roles of BCL-X_L. Our structural insights suggest that its high selectivity for BCL-X_L arises from a remarkable induced fit between the benzothiazole core and the hydrophobic groove of BCL-X_L. Specifically, the structures reveal remodelling and deepening of the P2 hydrophobic pocket in a manner distinct from that induced by the binding of ABT-737²⁹ and more extensive than that produced by binding of several natural BH3 peptides⁴. As our initial hit, compound **1a**, arose from a high-throughput screening campaign, our work highlights the value of diversity in a chemical screening library and suggests that other molecular scaffolds may be found with different binding profiles that may well be distinct from those of the BH3-only proteins.

Finally, our study clearly demonstrates that **WEHI-539** induces a robust apoptotic response *via* an on-target mechanism. We have used diverse genetically engineered cell lines to show that it satisfies the key criteria of authentic BH3-only protein mimicry⁴. Thus, **WEHI-539** not only binds very tightly to BCL-X_L, with IC₅₀ and K_D values close to or below 1 nM and a very slow dissociation rate, but it also invokes apoptotic responses that depend on BAX and/or BAK; furthermore, its biological activity is related to its binding profile, as elevated levels of MCL-1, BCL-2 and BCL-W confer marked resistance (**Supplementary Fig. 12**), and its ability to destroy platelets is a well-validated marker of

on-target BCL-X_L inhibition^{42,45}. In addition, **WEHI-539** induces a preferentially BAK-dependent apoptotic response in MEFs by selectively inhibiting BCL-X_L. Altogether, our structural, biochemical and cellular characterization of this series establish that these compounds kill cells by binding to and inhibiting BCL-X_L. Our work, therefore, describes the development of a valuable novel molecular probe that will provide an important tool for the study of BCL-X_L function in normal cells as well as in cancer development and maintenance. The findings thus constitute a major advance not only in the development of BH3 mimetics but also towards the broader goal of developing a molecular tool kit to target key protein-protein interactions.

Acknowledgments

The authors thank J Blyth, D Buczek, A Georgiou, H Ierino, C Rye, G Siciliano, G Thompson, A Wardak for outstanding technical assistance; S Cory, L Chen, MF van Delft, V Dixit, WD Fairlie, M Hijnen, S Hymowitz, E Lee, D Segal, A Strasser, V Tsui, AH Wei, W Welch, I Wertz for reagents and discussions throughout the project; P Pilling and V Streltsov (CSIRO, Australia) for their help with collecting data for compound **2** as well as the staff at the photon Factory BL6; and Abbvie for providing ABT-737. This work was supported by fellowships and grants from the Australian Research Council (ARC) (fellowship to PEC), the National Health and Medical Research Council (NHMRC) (fellowships to JMA, JBB, PMC, DCSH; development grant 305536; program grants 257502, 461221, 1016701), the Leukemia and Lymphoma Society (LLS) (SCORs 7015, 7413), the Cancer Council of Victoria (fellowship to PMC; grant-in-aid 461239) and the Australian Cancer Research Foundation. Infrastructure support from the NHMRC IRISS grant #361646 and a Victorian State Government OIS grant is gratefully acknowledged.

Competing financial information

Details for authors competing financial information is provided on the Nature Chemical Biology Web site.

Author contributions

GL: synthetic strategies, synthesized compounds, supervised the chemistry team, wrote manuscript.

PEC: X-ray crystallization, solved and analyzed structures; BES, KZ, WJAK, SK, KD: designed and

synthesized compounds; JMA: conceived study, analyzed data and results; JBB, KD, JAF, KGW:

designed synthetic strategies and oversaw chemistry efforts; PMC: conceived study, designed and

oversaw structural studies; KNL: performed biological experiments; PG, BJS: computational modeling;

WJF, JAF: designed studies and data analysis; RMM, JPP, IPS: HTCS campaign; HY: performed

Biacore experiments; DCSH: conceived study, designed and oversaw biological experiments, wrote manuscript.

Additional information

Supplementary information and synthesis of compounds **2, 3, 4, 5, 6** and **WEHI-539**.

FIGURE LEGENDS

Figure 1. Compounds from the benzothiazole series adopt a unique binding mode in BCL-X_L hydrophobic pocket P2.

- (a) Compound **1a** identified from the screen and close analog **1b**.
 - (b) Two potential binding modes for compound **1b** in the hydrophobic groove of BCL-X_L.
 - (c) Structure of compound **2**.
 - (d) Details of binding mode of compound **2** in the BCL-X_L hydrophobic groove, showing the benzothiazole moiety in the P2 pocket and the distinctive position of PHE105.
 - (e) Details of interaction network between the benzothiazole moiety of compound **2** and amino acid residues SER106, ASP107 and LEU108 in the P2 pocket.
 - (f) Position of PHE105 in relation to the furan moiety of compound **2** and the electrostatic interaction between ARG139 and the acylsulfonamide group of compound **2**.
- Dotted lines in panels (e) and (f) represent hydrogen bonds with their measured lengths in Å.

Figure 2. Core optimization and extension toward P4 augment affinity.

(a) Structures of compounds **3,4** with optimized cores and **5** and **6** with extension into the P4 pocket.

(b) X-ray crystal structure of compound **3** within the hydrophobic groove of BCL-X_L. In this structure, ARG132 interacts with a sulfate ion from the crystallization buffer and folds back above compound **3**.

(c) X-ray crystal structures of compounds **6** in complex with BCL-X_L.

Figure 3. WEHI-539 makes further interactions with residues in the P4 pocket and adopts a distinct binding mode compared to ABT-737.

(a) Structures of **WEHI-539**.

(b) X-ray crystal structures of **WEHI-539** in complex with BCL-X_L.

(c) Details of residues surrounding the benzylamino group of **WEHI-539** at the edge of the P4 pocket.

(d) Overlay of ABT-737 and **WEHI-539** bound to BCL-X_L. In blue: **WEHI-539**•BCL-X_L complex. In yellow: ABT-737•BCL-X_L complex. With both compounds, ARG139 is shown with a grey backbone.

Dotted lines in panels (c) (d) represent hydrogen bonds with their measured lengths in Å.

Figure 4. Decreased dissociation rate of the benzothiazole compounds from BCL-X_L underpins their increase in binding potency.

Representative sensorgrams recorded by Surface Plasmon Resonance for compounds **1b** (a), **3** (b), **5** (c), **WEHI-539** (d) and **ABT-737** (e). Sensorgrams representing direct binding kinetics for the indicated compounds are shown as Resonance Unit levels (RU, y-axis) as a function of time (s, x-axis) with increasing concentration (see experimental details in Online Methods and **Supplementary Note 1**).

(f) Compounds **1b**, **2**, **3**, **4**, **5**, **WEHI-539**, **ABT-737** and a 26-mer BIM-BH3 peptide are represented on the kinetic plots obtained from measurements of association and dissociation rates by direct binding assays using Surface Plasmon Resonance. x-axis: association rate; y-axis: dissociation rate. The parallel dotted lines on the kinetic plots represent lines of equipotency (K_D). Kinetic data are the average of at least 2 independent experiments.

Figure 5. WEHI-539 kills mouse embryonic fibroblasts (MEFs) only when MCL-1 is absent or blocked.

(a) Wild-type (WT), *mcl-1*^{-/-}, *bcl-2*^{-/-} or *bcl-x*^{-/-} MEFs were treated with 10 μ M **WEHI-539** or ABT-737 for 1 h and fractionated into mitochondrial-enriched (pellet) and cytosolic (soluble) fractions, which were subjected to SDS-gel electrophoresis and immunoblotted for cytochrome *c*; HSP70 was used as a loading control.

(b) The indicated MEFs were incubated for 4 h with 1 μ M **WEHI-539** or ABT-737 before assessing caspase-3 cleavage by immunoblotting SDS-gels.

(c) *mcl-1*^{-/-} MEFs and control (*mcl-1*^{wt/wt}) line were treated for 24 h with increasing concentrations of compound **3**, **5**, **WEHI-539** or ABT-737 in the presence of 1% FCS, and their viability determined by PI exclusion. Data are means \pm SEM of 3 independent experiments performed in triplicates.

(d) Robust correlation of cell killing with improved binding affinity. Correlation of kinetic K_D values of binding for BCL-X_L determined by SPR, direct binding assay (**Table 3**) and EC_{50} in *mcl-1*^{-/-} MEFs (1% FCS).

Figure 6. WEHI-539 provokes BAX/BAK mediated apoptosis on BCL-X_L dependent cells.

(a) Differential control of BAX and BAK by the pro-survival proteins in MCL-1 deficient cells³⁹.

(b) *bak*^{-/-}, *bax*^{-/-} and *bak*^{-/-}*bax*^{-/-} MEFs expressing the MCL-1-selective BH3 peptide, BIM2A, were treated with increasing doses of **WEHI-539** or ABT-737 for 24 h in triplicate and their viability assessed by PI exclusion.

(c) *Bak*^{-/-}, *bax*^{-/-} or *bak*^{-/-}*bax*^{-/-} MEFs expressing BIM2A were incubated for 4 hours with 1 μ M **WEHI-539** or ABT-737 and caspase-3 cleavage assessed by immunoblots after SDS-gel electrophoresis.

(d) *bak*^{-/-}, *bax*^{-/-} or *bak*^{-/-}*bax*^{-/-} MEFs expressing Bim2A were treated with 10 μ M **WEHI-539** or ABT-737 for 1 hr, fractionated into mitochondrial (pellet) and cytosolic (soluble) fractions, subjected to SDS-gel electrophoresis, and immunoblotted for cytochrome *c*. HSP70 was used as a loading control.

(e) Platelets from *bak*^{+/+}*bax*^{+/+} (n = 5) and *bak*^{-/-}*bax*^{+/+} (n = 5) mice were treated with increasing concentrations of **WEHI-539** or ABT-737 for 24 h. Non-linear regression analysis was used to calculate EC₅₀ values. Bars indicate mean EC₅₀ \pm SEM. *p* Values were calculated using unpaired, two-tailed Student's t-test (***p* = 0.006, ****p* = 0.0003).

(f) Pooled human platelets were pre-treated with or without qVD-OPH (Q-VD, 50 μ M, 10 min) then exposed to increasing concentrations of **WEHI-539** or ABT-737 (in 10% final plasma concentration) for 24 h in triplicate.

Data in (b), (e) and (f) are the mean EC₅₀ \pm SEM of 3 independent experiments performed in triplicate.

ONLINE METHODS

AlphaScreen™ Assay (Perkin Elmer)

GST-BCL-W (Δ C29), GST-BCL-X_L (Δ C25) and GST-MCL-1 (mouse/human chimera, Δ N151, Δ C25⁴⁶) were prepared as described^{35,46}, except that the proteins were eluted from glutathione-sepharose with glutathione before gel filtration purification. They were stored at -80°C. The biotinylated-Bak and biotinylated-Bim 26-mer peptides were obtained from Auspep and stored as 500 μ M stock solutions in DMSO (from AnalaR) at -20°C. The AlphaScreen™ GST (Glutathione-S-Transferase) detection kits were from Perkin Elmer Lifesciences. White, 384-well, low-volume assay plates and polypropylene, 384-well, compound storage plates were from Greiner Bio One and Matrical, respectively. Optical-grade, adhesive plate seals for assay plates were from Applied Biosystems and adhesive aluminum foil seals for compound plate storage from Beckman-Coulter.

The assay buffer (Stock 50 mM HEPES/100 mM NaCl, pH 7.5) was prepared fresh daily and adjusted to 5 mM DTT (1M stock aliquots stored at -20°C), casein (0.1 mg/mL sodium salt; aliquots stored at -20°C) and Tween 20 such that the “working assay buffer” contained 50 mM Hepes, 10 mM DTT, 100 mM NaCl, 0.05% Tween20 and 0.1 mg/mL casein, pH 7.4. Compounds were screened using the AlphaScreen GST (glutathione S-transferase) detection kit system. They were titrated into the working assay buffer (final DMSO concentration in the assay was 1.0% (v/v) in 384-well plates, which contained 0.6 nM (final well concentration) GST-tagged BCL-X_L Δ C25 protein, 5.0 nM (final well concentration) biotinylated Bim BH3-26mer peptide (Biotin-DLRPEIRIAQELRRIGDEFNETYTRR), and anti-GST coated acceptor beads and streptavidin-coated donor beads (both bead types at a final well concentration of 15 μ g/mL, diluted using “bead buffer” containing 50 mM Tris-HCl, pH 7.5, 0.01% Tween20 and 0.1 mg/mL casein); the assays were incubated at room temperature (RT) for 4 h before reading. More specifically: (i) each 384-well plate was prepared with 4.75 μ L of working Assay buffer and 0.25 μ L of compound stock (20 mM in DMSO) per well; (ii) binding partners were mixed using a 1:1 volumetric ratio; one tube contained BCL-X_L and the acceptor beads, while another contained the biotinylated BH3 peptide and the donor beads; (iii) both pairs of binding partners were preincubated for 30 min; (iv) 10 μ L of the acceptor beads/BCL-X_L complex was then added to all the wells of white Optiplates; (v) plates were covered and incubated at RT for another 30 min; (vi) 10 μ L of the donor bead/BH3 peptide complex was then added to each well; (vii) plates were sealed with aluminum foils and

incubated for a further 4 h at RT and then read using a PerkinElmer Fusion Alpha plate reader (Ex680, Em520-620 nM).

Cell lines and cell culture

All murine embryonic fibroblasts (MEFs) were from mice on a C57BL/6 background or backcrossed > 10 generations. MEFs were generated from E13–14.5 embryos and immortalized at passage 2–4 with SV40 large T antigen. *mcl-1^{-/-}*, *bcl-x^{-/-}*, *bak^{-/-}*, *bax^{-/-}*, *bak^{-/-}bax^{+/-}* and *bak^{-/-}bax^{-/-}* MEFs have been described^{40,47,48}. MEFs were cultured in Dulbecco's modified Eagles medium (DME) supplemented with 10% heat-inactivated fetal calf serum (FCS), 50 μ M 2-mercaptoethanol and 250 μ M asparagine in a humidified incubator at 37°C and 5% CO₂. Phoenix Ecotropic packaging cells were cultured in Dulbecco's Modified Eagles (DME) medium supplemented with 10% FCS.

Expression constructs and retroviral infection

Retroviral expression constructs containing FLAG-tagged human MCL-1, BCL-2 and BCL-X_L in the pMIH vector and the BCL-X_L short hairpin in the LMP vector have been described⁴⁸, as has the pMIH Bim2A construct⁴⁰. Retroviral expression constructs containing NOXA and NOXA3E have been previously described³⁵. All constructs were verified by sequencing and details are available from the authors. Retroviral constructs were transiently transfected into Phoenix Ecotropic packaging cells and viral supernatants used to infect target cells as described³⁵. The antibiotic resistant (hygromycin or puromycin) cells were expanded. Transgene expression or knockdown was confirmed by flow cytometric analysis or immunoblotting.

Cell killing assays

For flow cytometric analysis of cell viability, 1×10^4 cells were seeded into 24-well plates. The next day, fresh medium containing either 1% or 10% FCS and test compounds were added. In some experiments, cells were cultured in the presence of 50 mM qVD.OPh (Enzyme Systems). After incubation for 24 h, cell viability was quantified by propidium iodide (5 μ g/mL) exclusion using a FACScan[®] (BD). Eleven-point compound titration assays were performed by treating cells

(4×10^3) for 24 h in 96-well plates. Cytotoxicity was determined using CellTiter Glo® (Promega) and calculated as a percentage of a DMSO control.

Immunoblotting

Cells were lysed in lysis buffer (20 mM Tris, 135 mM NaCl, 1.5 mM MgCl₂, 1 mM EGTA, 10% glycerol and 1% Triton-X), supplemented with complete EDTA-free protease inhibitor cocktail (Roche). Proteins were resolved by SDS:PAGE (Novex gels; Invitrogen) and immunoblotted using anti-cytochrome C (7H8.2C12; BD Pharmingen), anti-caspase 3 (585; gift of Y. Lazebnik), anti-cleaved p17 fragment of caspase 3 (AB3623; Chemicon) and anti-HSP70 (N6; W. Welch, UCSF). Secondary antibodies included HRP-conjugated anti-mouse (Jackson ImmunoResearch) and anti-rabbit (Southern Biotech). Proteins were detected by enhanced chemiluminescence (GE Healthcare).

***In vitro* cytochrome c release**

Cell pellets were lysed in buffer (20 mM Hepes pH 7.2, 100 mM KCl, 5 mM MgCl₂, 1 mM EDTA, 1 mM EGTA, 250 mM Sucrose) containing 0.025% digitonin and protease inhibitors (Roche). Crude lysates containing mitochondria were incubated with 10 μM compound for 1 h at 30°C before pelleting. The supernatant was retained as the soluble fraction and the pellet lysed in Onyx buffer. Samples were analyzed by immunoblotting.

Platelet preparation and viability assays

Blood was obtained from age- and sex-matched C57BL/6 *bak^{+/+}bax^{+/+}* (n = 5) and C57BL/6 *bak^{-/-}bax^{-/-}* (n = 5) mice by cardiac puncture and collected in 0.1 volume Aster Jandl anticoagulant (85 mM sodium citrate, 69 mM citric acid, 20 mg/mL glucose, pH 4.6). Platelet rich plasma (PRP) was prepared by centrifugation and diluted 1:10 in Tyrodes buffer (137 mM NaCl, 2.7 mM KCl, 5 mM Hepes, 1 mM MgCl₂, 3 mM NaH₂PO₄, 5.5 mM dextrose, pH 7.35). Pooled human platelets, kindly provided by the Australian Red Cross Blood Service, were diluted 1:10 in Tyrodes buffer. Where indicated, platelets were pre-incubated with 50 μM qVD.OPh (Enzyme Systems) for 10 min. Compounds were incubated with platelets at 37°C for 24 h. Platelet viability was determined by CellTiterGlo® (Promega) and calculated as a percentage of a DMSO-treated control.

Fluorescent Polarization (FP, Supplementary Table 2)

The FP assay was used to measure the affinity of the compounds against GST-BCL-X_L, GST-Mcl-1 and GST-BCL-W using fluorescein-labeled peptides as a probe. The total volume of the FP assay was 25 μ L. The assay was carried out in 384-well format. Fluorescein-labeled peptide stock solution and protein stock solution were first prepared separately.

Fluorescein-labeled peptide stock solution: 8 nM of the fluorescein-labeled mutant BIM peptide [DLRPEIRIAQK(FAM)LRRIGDEFNE], in buffer comprised of 1 mM EDTA, 50 mM NaCl, 0.05% pluronic F-68, and 0.01% γ -globulin bovine in 20 mM phosphate buffer, pH 7.4.

Protein stock: 60 nM of GST-BCL-X_L in the same buffer as above.

For each compound, 12.5 μ l of protein stock solution was placed into each of eleven wells of a 384-well plate. To each well, compound was added such that final concentrations of 120, 60, 30, 15, 7.5, 3.75, 1.9, 0.95, 0.5, 0.25, 0.125 μ M were achieved. After 30 min incubation, 12.5 μ l of Fluorescein-labeled peptide stock solution was added into each well. The total DMSO concentration in each well was then adjusted to 4%. A free fluorescence peptide control (4 nM BIM peptide, 4% DMSO in buffer) and total binding control (4 nM BIM peptide, 30 nM BCL-X_L, 4% DMSO in buffer) were used to determine the free peptide and total binding polarization values, respectively for the assay. For GST-MCL-1, the final protein concentration was 80 nM. For GST-BCL-W, the final protein concentration was 12 nM.

For the assay using F-BAK [(FAM)-GQVGRQLAIIGDDINR] and GST-BCL-X_L, the final F-BAK concentration was 30 nM, the final GST-BCL-X_L concentration was 130 nM.

The 384 well plate was shaken for 5min and incubated at room temperature for 1 h and the polarization was measured at room temperature in a Envision (Perkin Elmer) plate reader with excitation at 480 nm and emission at 535 nm. IC₅₀ values were obtained by non-linear least squares fitting of the data to XLfit3 equation 205: $y=A+((B-A)/(1+((C/x)^D)))$.

Surface Plasmon Resonance Assays

1. Biacore 3000 (Supplementary Table 3)

Experiments were performed as described by Chen *et al.*³⁵. Pro-survival proteins (5 nM for BCL-X_L, BCL-W and MCL-1; 10 nM for BCL-2), with increasing concentrations of compound, were injected onto a CM5 chip bearing either a wildtype 26 mer BIM-BH3 or an inert BIM-BH3 mutant

peptide (BIM4E) peptides. Specific BIMBH3 binding responses were derived by subtracting the response of the BIM4E channel from the BIMBH3 channel. IC₅₀ values were calculated with Prism (GraphPad Software). Values are presented as an IC₅₀ in nM, with S.D. (n = 3 independent experiments). BCL-2, BCL-X_L and BCL-W were prepared as described by Chen *et al.*³⁵, MCL-1 was prepared as described by Czabotar *et al.*⁴⁶.

2. Direct binding assay (Biacore S51, Supplementary Tables 3 and Supplementary Note 1)

2.2 Method for potent binders ($K_d < 5$ nM)

Immobilization of anti-GST antibody: Anti-GST antibody surfaces were prepared by using standard amine-coupling procedures as instructed by the GST Capture Kit from Biacore. The running buffer contained 10 mM NaH₂PO₄•H₂O, 40 mM Na₂HPO₄•2H₂O, 150 mM NaCl, 1.0 mM EDTA, 0.03% Tween 20, 5% DMSO, pH 7.4. Flow cells (both spot 1 and spot 2) were activated by injecting 200 μ L of (11.5 mg/mL) NHS and EDC (75 mg/mL). 75 μ L of anti-GST antibody (30 μ g/mL) in 15 mM sodium acetate pH 5.0 was coupled *via* injection for 10 min at 5 μ L/min, followed by the injection of 175 μ L Ethanolamine (1 M) to deactivate residual amines. Finally, injection for 36 s of Biadesorb1 solution (0.5% SDS) and 40 s of Biadesorb2 solution (50 mM glycine pH 9.5) at 30 μ L/min at the end of the run. These resulted in about 10,000 RU of anti-GST antibody immobilized.

Capture of GST-BCL-X_L: The running buffer utilised was the same as for immobilization of anti-GST antibody. GST-BCL-X_L (0.1 mg/mL to 0.2 mg/mL) in the running buffer was injected at 10 μ L/min for 3 min across spot 2 only *via* hydrodynamic addressing, resulting in the capture of about 1200 RU protein.

Kinetic Analysis of potent small molecules and GST-BCL-X_L Interactions: A concentration series of each compound was injected at a flow rate of 90 μ L/min over three spots (spot 1: immobilized with anti-GST antibody only, spot 2: immobilized with GST-BCL-X_L captured by the anti-GST antibody, spot r: free/blank) at 25°C. The times allowed for compound association time and dissociation within the flow cell time were 2 min and 8 min, respectively. The buffer blank was also injected periodically for double referencing along with buffer samples containing an incremental range of 4% – 6 % DMSO, used for solvent correction. The antibody surface was regenerated between binding cycles with 40 s injection of 10 mM glycine-HCl, pH 2.2. The protein was injected at 10 μ L/min for 3 min across spot 2 only at the beginning of each cycle.

Data Analysis: All sensorgrams were processed by using double referencing:

1. The response from the control spot (spot 1) was subtracted from the binding response (spot 2), followed by solvent correction.
2. The response from an average of buffer injections was subtracted.

To obtain kinetic rate constants (k_a and k_d), corrected response data were then fitted to a one-to-one binding site model using local fit, which includes correction for mass transport limitations. The equilibrium dissociation constant (K_d) was determined by k_d/k_a .

2.2 Methods for weaker binders ($K_d > 5$ nM)

Immobilization of anti-GST antibody: The anti-GST antibody was immobilized on both spot 1 and spot 2 of the same flow cell similar to the method used was similar to the one described for tight binders.

Capture of GST-BCL-X_L: The GST-BCL-X_L (about 1300 RU) was captured on both spot 1 and spot 2 of the same flow cell using a method similar to the one described for tight binders.

Kinetic Analysis of non-potent small molecules and GST-BCL-X_L Interactions: 30 nM of 26-mer-wt-BIM (30 μ L/min x 1 min) was injected into spot 1 only at the beginning of each cycle using hydrodynamic addressing, resulting in the BCL-X_L BH3 binding groove being “pre-blocked” with wt-BIM 26-mer peptide. A concentration series of each compound was injected at a flow rate of 90 μ L/min over three spots (spot 1: loaded with GST-BCL-X_L and BIM peptide, spot 2: loaded with GST-BCL-X_L, spot r: free) at 25°C. The association and dissociation measurement time periods for compounds were 60 and 160 s, respectively. The buffer blank was also injected periodically for double referencing along with buffer samples containing 4% – 6% DMSO used for solvent correction. The sensorgrams of (spot 1 –r) reflected the non-specific binding to captured GST-BCL-X_L protein, as the BH3 binding groove had been “pre-blocked” with wt-BIMBH3 26 mer peptide. The sensorgrams of (spot 2 – spot 1) reflected the resultant specific binding to the GST-BCL-X_L protein’s binding groove (prior to DMSO solvent correction).

Data Analysis: The same method described for tight binders was used.

3. Direct binding assay Biacore 4000 (Supplementary Table 3 and Supplementary Note 1)

Immobilization of anti-GST antibody: Anti-GST antibody surfaces were prepared as described above for the Biacore S51 experiments. GST-A1 (mouse DC-20 with 2 mutations P104K and C113S) was prepared as described⁴⁹.

Capture of GST-BCL-X_L, GST-BCL-W, GST-MCL-1 and GST-A1: capture of these 4 pro-survival constructs were performed as described above for the Biacore S51 experiments.

Immobilization of His-BCL2: His-Bcl-2 assays were performed utilizing a Nickel chip. The nitrilotriacetic acid (NTA) pre-immobilized on a carboxymethylated dextran matrix was saturated with nickel by a three minute injection of 500 μ M of NiCl₂. A flow rate of 30 μ L/min was used. The chip surface was activated by a 10 minute injection of 0.2 M EDC, 50 mM NHS at 15 μ L/min. His-Bcl-2 (0.010 mg/mL) was subsequently immobilized on the chip surface by injection at 10 μ L/min for 10 minutes. The running buffer consisted of 0.01 M HEPES, 0.15 M NaCl, 50 μ M EDTA and 0.05% P20 at pH7.4. The unreacted succinimide esters were inactivated by an injection of 140 μ L of 1M Ethanolamine at pH8.5. The non-covalently bound proteins were removed with running buffer. This method enabled immobilization of 4000 to 5000RU of His-Bcl-2 protein.

The “Pre-blocking” strategy of pro-survival proteins with BIMBH3 was not used in these experiments. Analysis was therefore performed from a spot loaded with a pro-survival protein substracted with a blank reference spot.

Kinetic Analysis of WEHI-539/GST-BCL-X_L Interactions: the protocol for tight binders described above (Biacore S51 assay set-up) was followed with a flow rate of 30 μ L/min.

Kinetic Analysis of WEHI-539 and mut-BIMBH3 against GST-BCL-X_L, GST-BCL-W, GST-MCL-1 and GST-A1 interactions: the protocol for weak binders described above (Biacore S51 assay set-up) was followed with a flow rate of 30 μ L/min.

Kinetic Analysis of WEHI-539 and mut-BIMBH3 against His-BCL-2: The analysis of the interaction between small molecules and His-Bcl-2 protein was performed in a similar fashion to the previously described GST tagged proteins. For His-Bcl-2 protein assays, the running buffer consisted of 0.01M HEPES, 0.15 M NaCl, 50 μ M EDTA, 0.05%P20 and 1% DMSO at pH7.4. The his-Bcl-2 protein surface was regenerated between binding cycles with at least 5 minutes

injection of running buffer for tight binding compounds. Compounds were injected at varying concentrations with a flow rate of 30 $\mu\text{L}/\text{min}$.

Kinetic data were analysed using a 1:1 model and local curve fit.

Gel Filtration of BCL-X_L•compound 2 complex for size determination (Supplementary Fig. 2)

A sample of BCL-X_L bound to compound 2 was prepared in a similar manner to that used for sample preparation for crystallisation. Protein at 0.24 mg/mL was incubated with a 1.5 fold molar excess of compound 2 and concentrated to 24 mg/mL using a 10 kDa cut-off centrifugal concentrator. Samples were subjected to size exclusion chromatography using a Superdex75 (10/300) column with TBS (20 mM Tris pH 8.0, 150 mM NaCl) as running buffer.

X-ray Crystallography (supplementary Table 4)

Crystallography for structures of BCL-X_L in complex with compounds was based on the method used to crystallize BCL-X_L in complex with ABT-737²⁹. Briefly, complexes were prepared by mixing protein and compound at low concentration (0.2 - 0.5 mg/mL of protein). For compounds 2, 3 and 6 the BCL-X_L construct used contained a shortened $\alpha 1$ - $\alpha 2$ loop and a C-terminal truncation ($\Delta 45$ -84, $\Delta C25$)⁵⁰. For **WEHI-539** the construct contained a larger truncation in the $\alpha 1$ - $\alpha 2$ loop ($\Delta 27$ -82, $\Delta C24$)⁵¹. Samples were concentrated and buffer exchanged twice with TBS to remove residual DMSO in which the compounds had been dissolved. Samples were crystallized at 293K in hanging drops using well solutions containing (NH₄)₂SO₄ (1.6 - 2.2 M) in buffers ranging from pH 5.5 to 8.0. For compound 3 the well solution also contained 0.2 M Mg₂SO₄. Crystals were frozen in well solution supplemented with 25 % ethylene glycol and data collected at 100 K using either an in-house RAXIS-IV++ detector with a micro-max007 X-ray source (compounds 3, 6 and **WEHI-539**), or at the photon factory BL6A (Compound 2). Data were processed with either HKL2000⁵² or XDS⁵³, solved by molecular replacement with PHASER⁵⁴, refinement performed with either REFMAC⁵⁵ or PHENIX⁵⁶ and model building performed with COOT⁵⁷.

Validation of BCL-X_L dependency of *mcl-1*^{-/-} MEF cell lines (Supplementary Figure 18)

Long term colony formation assays were performed by plating an equal number of retrovirally infected cells 24 h post-infection in medium containing appropriate antibiotics for selection. Medium and antibiotics was replaced at day 3. Colonies were stained with Giemsa and scored at day 7.

Summary of statistical analysis

GraphPad Prism® was used for all statistical analysis. Data are presented as mean ± Standard Error of the Mean (SEM) except where otherwise stated. Students t-test (unpaired, two-tailed) was used to calculate statistical significance. IC₅₀ and EC₅₀ values were calculated from sigmoidal dose response curves with variable slope.

Additional information

Information and data for Biacore assays, synthesis and characterization of compounds **2**, **3**, **4**, **5**, **6** and **WEHI-539** is presented in **Supplementary Notes**.

PDB database deposits

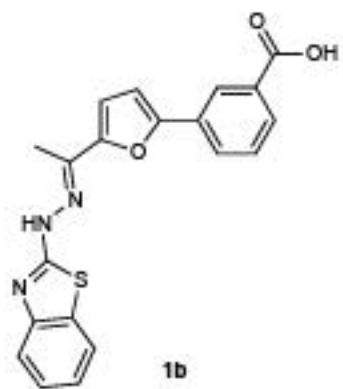
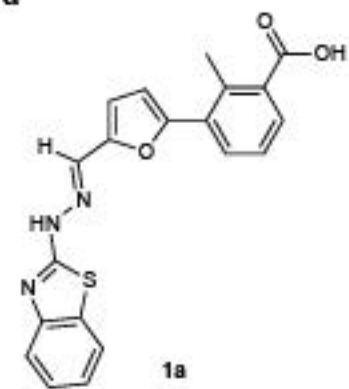
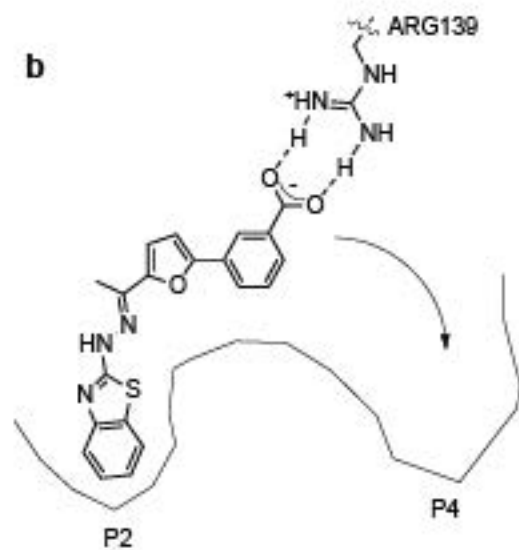
Compound Number	PDB accession code
Compound 2	3ZK6
Compound 3	3ZLN
Compound 6	3ZLO
WEHI-539	3ZLR

References

1. Hotchkiss, R.S., Strasser, A., McDunn, J.E. & Swanson, P.E. Cell death. *N. Engl. J. Med.* **361**, 1570-1583 (2009).
2. Strasser, A., Cory, S. & Adams, J.M. Deciphering the rules of programmed cell death to improve therapy of cancer and other diseases. *EMBO J.* **30**, 3667-3683 (2011).
3. Glaser, S.P. *et al.* Anti-apoptotic Mcl-1 is essential for the development and sustained growth of acute myeloid leukemia. *Genes Dev.* **26**, 120-125 (2012).
4. Lessene, G., Czabotar, P.E. & Colman, P.M. BCL-2 family antagonists for cancer therapy. *Nat. Rev. Drug Discov.* **7**, 989-1000 (2008).
5. Wells, J.A. & McClendon, C.L. Reaching for high-hanging fruit in drug discovery at protein-protein interfaces. *Nature* **450**, 1001-1009 (2007).
6. Mullard, A. Protein-protein interaction inhibitors get into the groove. *Nat. Rev. Drug Discov.* **11**, 173-175 (2012).
7. Beroukhim, R. *et al.* The landscape of somatic copy-number alteration across human cancers. *Nature* **463**, 899-905 (2010).
8. Amundson, S.A. *et al.* An informatics approach identifying markers of chemosensitivity in human cancer cell lines. *Cancer Res.* **60**, 6101-10 (2000).
9. Vaux, D.L., Cory, S. & Adams, J.M. Bcl-2 gene promotes haemopoietic cell survival and cooperates with c-myc to immortalize pre-B cells. *Nature* **335**, 440-2 (1988).
10. Strasser, A., Harris, A.W., Bath, M.L. & Cory, S. Novel primitive lymphoid tumours induced in transgenic mice by cooperation between myc and bcl-2. *Nature* **348**, 331-3 (1990).
11. Kelly, P.N. & Strasser, A. The role of Bcl-2 and its pro-survival relatives in tumourigenesis and cancer therapy. *Cell Death Differ.* **18**, 1414-24 (2011).
12. Lindsten, T. *et al.* The combined functions of proapoptotic Bcl-2 family members bak and bax are essential for normal development of multiple tissues. *Mol. Cell* **6**, 1389-99 (2000).
13. Leber, B., Lin, J. & Andrews, D.W. Still embedded together binding to membranes regulates Bcl-2 protein interactions. *Oncogene* **29**, 5221-30 (2010).
14. Leber, B., Lin, J. & Andrews, D.W. Embedded together: the life and death consequences of interaction of the Bcl-2 family with membranes. *Apoptosis* **12**, 897-911 (2007).
15. Labi, V., Grespi, F., Baumgartner, F. & Villunger, A. Targeting the Bcl-2-regulated apoptosis pathway by BH3 mimetics: a breakthrough in anticancer therapy? *Cell Death Differ.* **15**, 977-87 (2008).
16. Oltersdorf, T. *et al.* An inhibitor of Bcl-2 family proteins induces regression of solid tumours. *Nature* **435**, 677-681 (2005).
17. Rudin, C.M. *et al.* Phase II Study of Single-Agent Navitoclax (ABT-263) and Biomarker Correlates in Patients with Relapsed Small Cell Lung Cancer. *Clin. Cancer Res.* **18**, 3163-3169 (2012).
18. Gandhi, L. *et al.* Phase I study of navitoclax (ABT-263), a novel Bcl-2 family inhibitor, in patients with small-cell lung cancer and other solid tumors. *J. Clin. Oncol.* **29**, 909-16 (2011).
19. Roberts, A.W. *et al.* Substantial susceptibility of chronic lymphocytic leukemia to BCL2 inhibition: results of a phase I study of navitoclax in patients with relapsed or refractory disease. *J. Clin. Oncol.* **30**, 488-96 (2012).

20. Wilson, W.H. *et al.* Navitoclax, a targeted high-affinity inhibitor of BCL-2, in lymphoid malignancies: a phase 1 dose-escalation study of safety, pharmacokinetics, pharmacodynamics, and antitumour activity. *Lancet Oncol.* **11**, 1149-59 (2010).
21. Park, C.M. *et al.* Discovery of an orally bioavailable small molecule inhibitor of prosurvival B-cell lymphoma 2 proteins. *J. Med. Chem.* **51**, 6902-6915 (2008).
22. Tse, C. *et al.* ABT-263: a potent and orally bioavailable Bcl-2 family inhibitor. *Cancer Res.* **68**, 3421-8 (2008).
23. Souers, A.J. *et al.* ABT-199, a potent and selective BCL-2 inhibitor, achieves antitumor activity while sparing platelets. *Nat Med* (2013).
24. Mason, K.D. *et al.* Programmed anuclear cell death delimits platelet life span. *Cell* **128**, 1173-86 (2007).
25. Zhang, H. *et al.* Bcl-2 family proteins are essential for platelet survival. *Cell Death Differ.* **14**, 943-951 (2007).
26. Baell, J.B. & Holloway, G.A. New substructure filters for removal of pan assay interference compounds (PAINS) from screening libraries and for their exclusion in bioassays. *J. Med. Chem.* **53**, 2719-40 (2010).
27. Petros, A.M. *et al.* Rationale for Bcl-xL/Bad peptide complex formation from structure, mutagenesis, and biophysical studies. *Protein Sci.* **9**, 2528-2534 (2000).
28. Petros, A.M., Olejniczak, E.T. & Fesik, S.W. Structural biology of the Bcl-2 family of proteins. *Biochim. Biophys. Acta* **1644**, 83-94 (2004).
29. Lee, E.F. *et al.* Crystal structure of ABT-737 complexed with Bcl-x(L): implications for selectivity of antagonists of the Bcl-2 family. *Cell Death Differ.* **14**, 1711-1713 (2007).
30. Liu, X., Dai, S., Zhu, Y., Marrack, P. & Kappler, J. The structure of a Bcl-xL/Bim fragment complex: implications for Bim function. *Immunity* **19**, 341-352 (2003).
31. Oberstein, A., Jeffrey, P.D. & Shi, Y. Crystal structure of the Bcl-XL-Beclin 1 peptide complex: Beclin 1 is a novel BH3-only protein. *J. Biol. Chem.* **282**, 13123-32 (2007).
32. Sattler, M. *et al.* Structure of Bcl-xL-Bak peptide complex: recognition between regulators of apoptosis. *Science* **275**, 983-986 (1997).
33. Lee, E.F. *et al.* Conformational changes in Bcl-2 pro-survival proteins determine their capacity to bind ligands. *J. Biol. Chem.* **284**, 30508-17 (2009).
34. Wendt, M.D. *et al.* Discovery and structure-activity relationship of antagonists of B-cell lymphoma 2 family proteins with chemopotential activity in vitro and in vivo. *J. Med. Chem.* **49**, 1165-81 (2006).
35. Chen, L. *et al.* Differential targeting of prosurvival Bcl-2 proteins by their BH3-only ligands allows complementary apoptotic function. *Mol. Cell* **17**, 393-403 (2005).
36. Czabotar, P.E. & Lessene, G. Bcl-2 Family Proteins as Therapeutic Targets. *Curr. Pharm. Des.* **16**, 3132-3148 (2010).
37. van Delft, M.F. *et al.* The BH3 mimetic ABT-737 targets selective Bcl-2 proteins and efficiently induces apoptosis via Bak/Bax if Mcl-1 is neutralized. *Cancer Cell* **10**, 389-399 (2006).
38. van Delft, M.F. *et al.* The BH3 mimetic ABT-737 targets selective Bcl-2 proteins and efficiently induces apoptosis via Bak/Bax if Mcl-1 is neutralized. *Cancer Cell* **10**, 389-99 (2006).
39. Willis, S.N. *et al.* Proapoptotic Bak is sequestered by Mcl-1 and Bcl-xL, but not Bcl-2, until displaced by BH3-only proteins. *Genes Dev.* **19**, 1294-305 (2005).
40. Lee, E.F. *et al.* A novel BH3 ligand that selectively targets Mcl-1 reveals that apoptosis can proceed without Mcl-1 degradation. *J. Cell Biol.* **180**, 341-55 (2008).

41. Merino, D. *et al.* Bcl-2, Bcl-xL, and Bcl-w are not equivalent targets of ABT-737 and navitoclax (ABT-263) in lymphoid and leukemic cells. *Blood* **119**, 5807-16 (2012).
42. Josefsson, E.C. *et al.* Megakaryocytes possess a functional intrinsic apoptosis pathway that must be restrained to survive and produce platelets. *J. Exp. Med.* **208**, 2017-31 (2011).
43. Gleeson, M.P. Generation of a Set of Simple, Interpretable ADMET Rules of Thumb. *J. Med. Chem.* **51**, 817-834 (2008).
44. Shoemaker, A.R. *et al.* A small-molecule inhibitor of Bcl-X-L potentiates the activity of cytotoxic drugs in vitro and in vivo. *Cancer Res.* **66**, 8731-8739 (2006).
45. Mason, K.D. *et al.* The delicate balance between pro survival BCL XL and pro apoptotic BAK determines platelet life span. *Exp. Hematol.* **35**, 33-33 (2007).
46. Czabotar, P.E. *et al.* Structural insights into the degradation of Mcl-1 induced by BH3 domains. *Proc. Natl. Acad. Sci. USA* **104**, 6217-22 (2007).
47. Willis, S.N. *et al.* Apoptosis initiated when BH3 ligands engage multiple Bcl-2 homologs, not Bax or Bak. *Science* **315**, 856-859 (2007).
48. Fletcher, J.I. *et al.* Apoptosis is triggered when prosurvival Bcl-2 proteins cannot restrain Bax. *Proc. Natl. Acad. Sci. USA* **105**, 18081-7 (2008).
49. Smits, C., Czabotar, P.E., Hinds, M.G. & Day, C.L. Structural plasticity underpins promiscuous binding of the prosurvival protein A1. *Structure* **16**, 818-29 (2008).
50. Muchmore, S.W. *et al.* X-ray and NMR structure of human Bcl-xL, an inhibitor of programmed cell death. *Nature* **381**, 335-41 (1996).
51. Kvansakul, M. *et al.* Vaccinia virus anti-apoptotic F1L is a novel Bcl-2-like domain-swapped dimer that binds a highly selective subset of BH3-containing death ligands. *Cell Death Differ.* **15**, 1564-71 (2008).
52. Otwinowski, Z., Minor, W. & Charles W. Carter, Jr. Processing of X-ray diffraction data collected in oscillation mode. in *Methods in Enzymology*, Vol. Volume 276 307-326 (Academic Press, 1997).
53. Kabsch, W. Integration, scaling, space-group assignment and post-refinement. *Acta Crystallogr. D Biol. Crystallogr.* **66**, 133-44 (2010).
54. McCoy, A.J. *et al.* Phaser crystallographic software. *J. App. Cryst.* **40**, 658-674 (2007).
55. Murshudov, G.N., Vagin, A.A. & Dodson, E.J. Refinement of macromolecular structures by the maximum-likelihood method. *Acta Crystallogr. D Biol. Crystallogr.* **53**, 240-55 (1997).
56. Adams, P.D. *et al.* PHENIX: a comprehensive Python-based system for macromolecular structure solution. *Acta Crystallogr. D Biol. Crystallogr.* **66**, 213-21 (2010).
57. Emsley, P. & Cowtan, K. Coot: model-building tools for molecular graphics. *Acta Crystallogr. D Biol. Crystallogr.* **60**, 2126-32 (2004).

Fig. 1**a****b**

ARG139

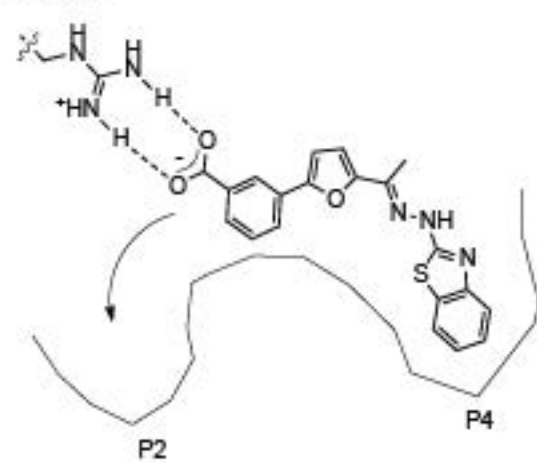
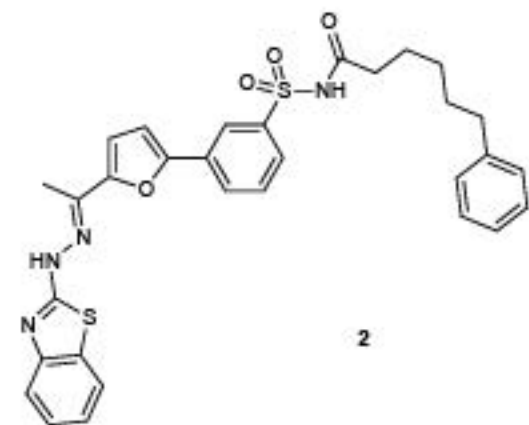
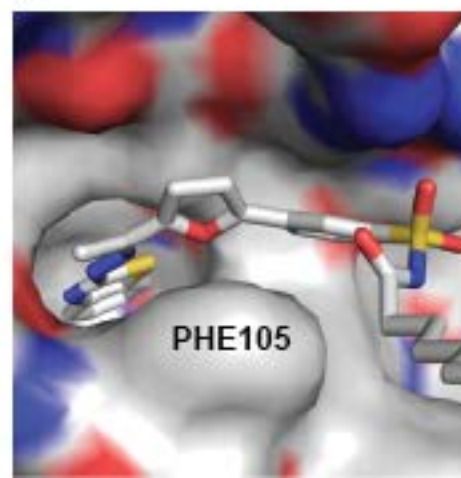
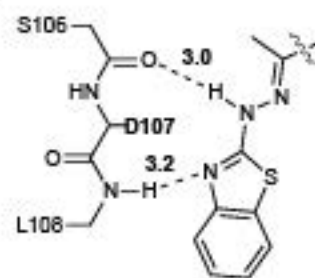
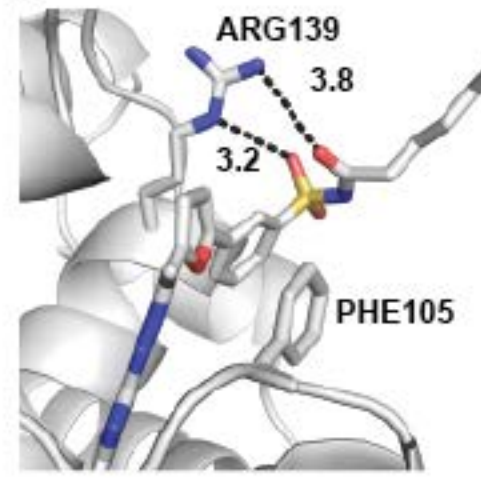
**c****d****e****f**

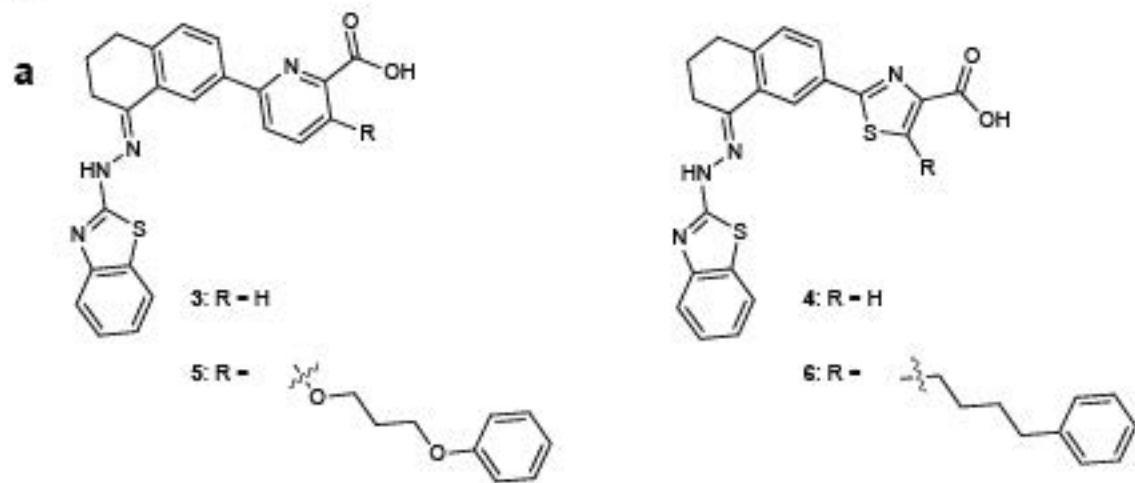
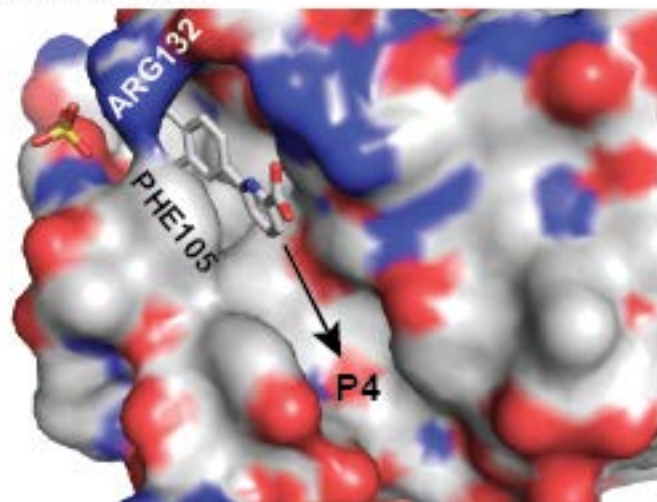
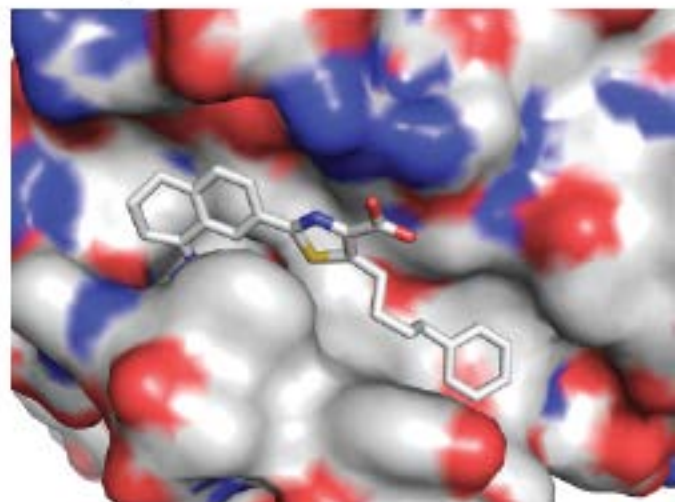
Fig. 2**b Compound 3****c Compound 6**

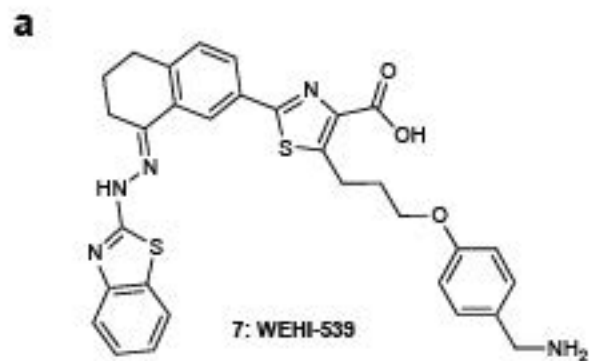
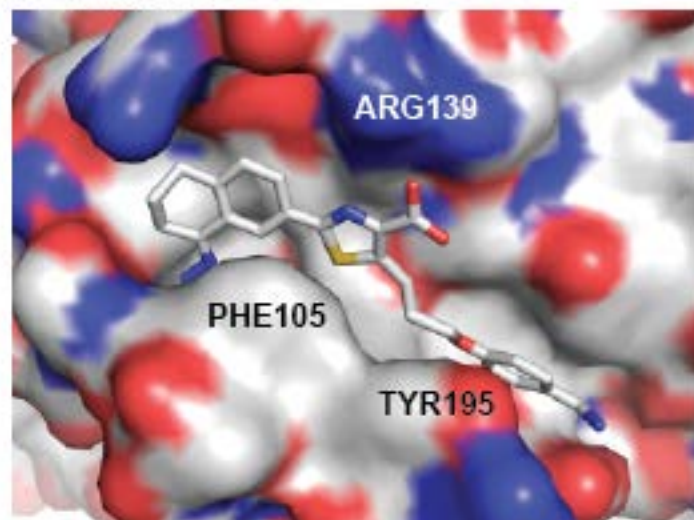
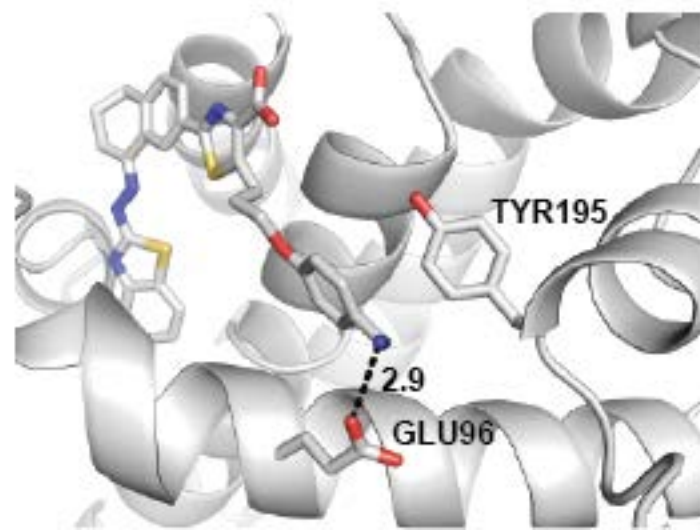
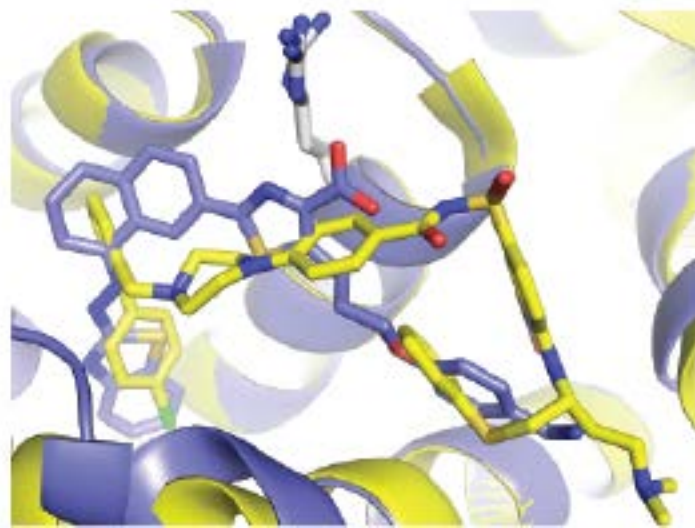
Fig. 3**b WEHI-539****c WEHI-539****d WEHI-539 and ABT-737**

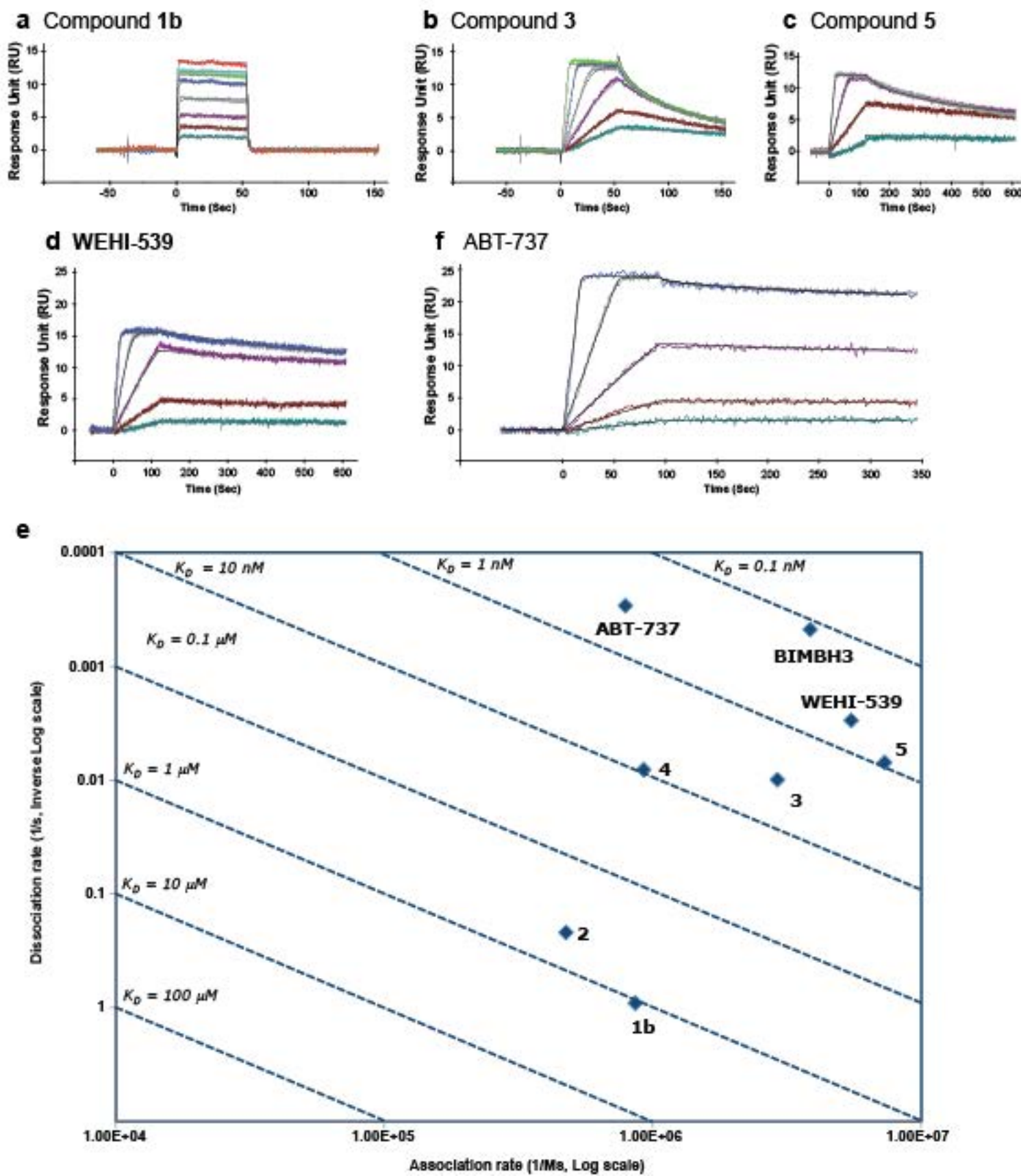
Fig. 4

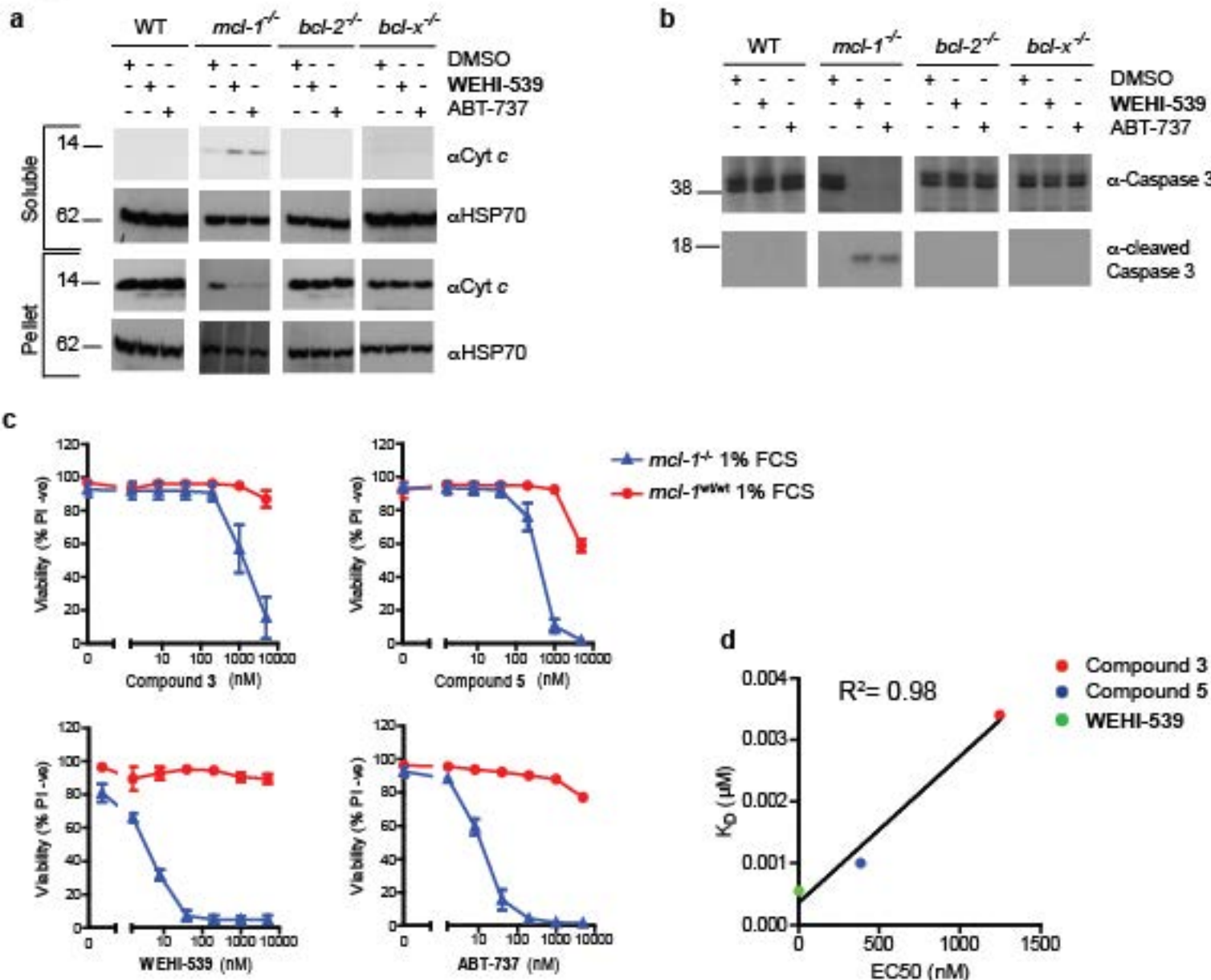
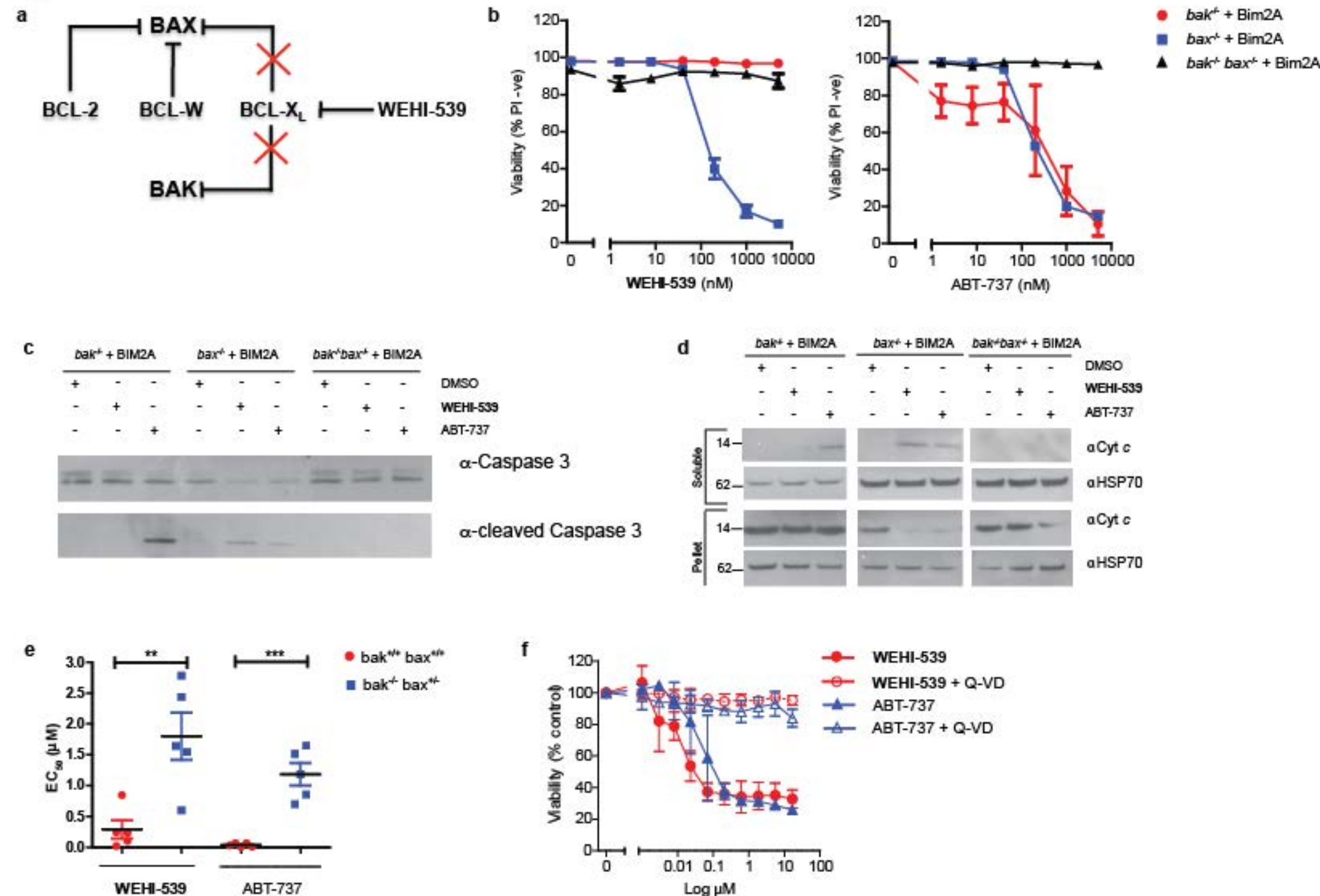
Fig. 5

Fig. 6

This is the authors' accepted version of their manuscript accepted for publication in Nature Chemical Biology.

The final publication is available at Nature Publishing Group :

Lessene G, Czabotar PE, Sleebs BE, Zobel K, Lowes KN, Adams JM, Baell JB, Colman PM, Deshayes K, Fairbrother WJ, Flygare JA, Gibbons P, Kersten WJA, Kulasegaram S, Moss RM, Parisot JP, Smith BJ, Street IP, Yang H, Huang DCS, Watson KG. Structure-guided design of a selective BCL-XL inhibitor. *Nature Chemical Biology*. 2013 9(6):390-397.
doi:10.1038/nchembio.1246